Dynamical Uncertainty Propagation with Noisy Quantum Parameters

Mogens Dalgaard,[1] Carrie A. Weidner,[1] and Felix Motzoi[2,*]
[1]Department of Physics and Astronomy, Aarhus University, Ny Munkegade 120, 8000 Aarhus C, Denmark
[2]Forschungszentrum Jülich, Institute of Quantum Control (PGI-8), D-52425 Jülich, Germany

(Received 26 August 2021; accepted 25 March 2022; published 13 April 2022)

Many quantum technologies rely on high-precision dynamics, which raises the question of how these are influenced by the experimental uncertainties that are always present in real-life settings. A standard approach in the literature to assess this is Monte Carlo sampling, which suffers from two major drawbacks. First, it is computationally expensive. Second, it does not reveal the effect that each individual uncertainty parameter has on the state of the system. In this Letter, we evade both these drawbacks by incorporating propagation of uncertainty directly into simulations of quantum dynamics, thereby obtaining a method that is orders of magnitude faster than Monte Carlo simulations and directly provides information on how each uncertainty parameter influences the system dynamics. Additionally, we compare our method to experimental results obtained using the IBM quantum computers.

DOI: 10.1103/PhysRevLett.128.150503

Technologies based on quantum information may lead to ground-breaking progress within numerical search [1], cryptography [2], simulation [3,4], optimization [5,6], and machine learning [7,8]. Realization of these technologies requires improvements in our ability to measure, design, build, and realistically model subparts of these quantum systems [9]. The latter necessitates the incorporation of experimental uncertainties that are omnipresent in real quantum systems into numerical simulations of such systems.

Propagation of uncertainty (or error) is a standard tool for understanding how experimental uncertainties transform in calculations [10]. Here we incorporate propagation of uncertainty into quantum dynamical simulation and characterization by drawing on methods from gradient-based quantum control theory [11–14]. We demonstrate a significant speed up relative to Monte Carlo sampling, which is the current standard in the literature (cf. Refs. [15–28] for recent examples).

Moreover, our method allows for in-depth analysis of how experimental uncertainties independently or cooperatively influence the dynamical observables in the system. This is valuable for investigating the consistency between models and experimental results, as well as the characterization of noise, uncertainty levels, and the influence of different experimental parameters. For example, within circuit QED we have, in recent years, seen improvements in one- and two-qubit gate operations due to better understanding and calibration of experimental systems [29–33]. Careful study of these systems' uncertainties and their influence on quantum dynamics is necessary to push this frontier further.

The methods proposed here apply also to the construction of composite control sequences specifically designed to perform robustly against fluctuations in the system parameters [34–37], as well as enhancing quantum control and optimization protocols [11,16,17,38–43]. That is, the sensitivity to parameter uncertainties can be maximized or minimized for tomographic reconstructions, system identification, and quantum metrology. For example, the presented method could aid physicists in designing quantum computation architectures [44–49]. These need to perform stably under smaller fluctuations in the system parameters, and as such, a detailed analysis of their performance under realistic and expected uncertainties could help assess a given architecture's robustness. We term our approach quantum uncertainty propagation in dynamics (QUPID).

Theory.—Let $Z(t)$ denote a function that depends on the evolution of the system, e.g., the expectation value of a Hermitian operator $Z(t) = \langle \hat{Z} \rangle$ or the Haar-averaged gate fidelity $Z(t) = \int_\psi \langle \psi | U(t)^\dagger U_{\text{target}} | \psi \rangle d\psi$. Now let the Hamiltonian operator and other system evolution variables depend on a set of normally distributed parameters $\boldsymbol{\theta} = (\theta_1, \theta_2, \ldots, \theta_M)$ with mean $\bar{\boldsymbol{\theta}} = (\overline{\theta_1}, \overline{\theta_2}, \ldots, \overline{\theta_M})$ and covariances $\sigma_{i,j} = \mathbb{E}[(\theta_i - \overline{\theta_i})(\theta_j - \overline{\theta_j})]$, which we assume are relatively small [50]. Here $\sigma_j^2 = \sigma_{j,j}$ denotes the variance. Thus, Z is a function of the parameters $\boldsymbol{\theta}$, which we may Taylor expand around the mean values $\bar{\boldsymbol{\theta}}$,

$$Z(\boldsymbol{\theta}, t) \simeq Z(\bar{\boldsymbol{\theta}}, t) + \sum_j \frac{\partial Z(\bar{\boldsymbol{\theta}}, t)}{\partial \theta_j} (\theta_j - \bar{\theta}_j) + \frac{1}{2} \sum_{i,j} \frac{\partial^2 Z(\bar{\boldsymbol{\theta}}, t)}{\partial \theta_i \partial \theta_j} (\theta_i - \bar{\theta}_i)(\theta_j - \bar{\theta}_j), \quad (1)$$

where truncating the Taylor expansion to second order is justified by assuming that the uncertainty in the system

parameters only induces small changes in Z (e.g., with small covariances). Under this assumption, evaluating the mean (as in the Supplemental Material [54]) reveals [51,52]

$$\mathbb{E}[Z(\boldsymbol{\theta},t)] \simeq Z(\bar{\boldsymbol{\theta}},t) + \frac{1}{2}\sum_{i,j}\frac{\partial^2 Z(\bar{\boldsymbol{\theta}},t)}{\partial\theta_i\partial\theta_j}\sigma_{i,j}, \tag{2}$$

informing us directly how uncertainties in the system dynamics may lead to shifts away from the expected value $Z(\bar{\boldsymbol{\theta}},t)$ at different times. For example, this term could cause a reduction in the predicted average gate fidelity. This is especially critical to analytical protocols for parameter estimation, where stochasticity in the parameter may modify the mean estimation. Consequently, the intuitive approach of assessing robustness via first derivatives will fail to capture the expected loss in average fidelity, as its effect will simply average to zero [52]. In the case that the uncertainties are statistically independent ($\sigma_{i,j} = 0$ if $i \neq j$), we can further see that the individual parameter uncertainties are additive, allowing them to be calculated individually by, e.g., Monte Carlo simulations, or more efficiently, as we show below, by propagation of uncertainty through the dynamics. Note, Eq. (2) works for all symmetric probability distributions. In the Supplemental Material [54], we generalize this result to any probability distribution and order of Taylor expansion [53].

A similar calculation for the variance yields

$$\begin{aligned}\mathrm{Var}[Z(\boldsymbol{\theta},t)] \simeq &\sum_{i,j}\frac{\partial Z(\bar{\boldsymbol{\theta}},t)}{\partial\theta_i}\frac{\partial Z(\bar{\boldsymbol{\theta}},t)}{\partial\theta_j}\sigma_{i,j} \\ &+\frac{1}{2}\sum_{i,j,k,l}\frac{\partial^2 Z(\bar{\boldsymbol{\theta}},t)}{\partial\theta_i\partial\theta_j}\frac{\partial^2 Z(\bar{\boldsymbol{\theta}},t)}{\partial\theta_k\partial\theta_l}\sigma_{i,k}\sigma_{j,l},\end{aligned} \tag{3}$$

which we detail in Ref. [54], commenting further on the truncation error in Eqs. (2) and (3). Now we sketch how to obtain the derivatives that appear in Eqs. (2) and (3) through analysis of the dynamics. Although this Letter focuses on quantum dynamics, our approach is also applicable to other areas (e.g., classical physics); we only require access to a model $Z(\boldsymbol{\theta},t)$ from which the derivatives are obtainable (numerically or analytically). To demonstrate this, we apply our method to a classical damped pendulum in the Supplemental Material [54].

To calculate the dynamical uncertainties in system observables with the above equations, it is necessary to efficiently propagate the equations of motion for the derivatives of these observables. To do this, we draw on established methods from the field of quantum optimal control theory [11–14]. There are several candidate methods to obtain the first and second-order derivatives [13,14,60–62]. We outline one approach based on matrix diagonalization [13,14] in the main text, and provide an alternative by finite difference [61] in the Supplemental Material [54,63]. We have so far tacitly assumed that Z was a functional of the current state of the system $\chi(t)$, which solves the dynamic equation of motion $(\partial/\partial t)\chi(t) = A(t)\chi(t)$. This could be, e.g., the Schrödinger equation $A(t) = -iH(t)$ with $\hbar = 1$ and χ being a single quantum state, a unitary operator, a collection of states, or a density matrix with evolution governed by the von Neumann or the Lindblad master equation (cf. Supplemental Material [54]).

We discretize the time evolution for a total duration T in N equidistant steps Δt and numerically solve the equation of motion using the time evolution operator $\chi_{n+1} = U_n\chi_n$, where $\chi(t_n) = \chi_n$ and $U_n = e^{A(t_n+\Delta t/2)}$ is the midpoint interpolation of the truncated Magnus series [66], leading to a global second order error in $\chi(T)$ that can be made arbitrarily small by suitable choice of Δt. The derivatives of Z ultimately depend on the derivative of χ, which give via the chain rule

$$\frac{\partial}{\partial\theta_j}\chi_{n+1} = \left(\frac{\partial}{\partial\theta_j}U_n\right)\chi_n + U_n\frac{\partial}{\partial\theta_j}\chi_n, \tag{4}$$

and similarly for the Hessian

$$\begin{aligned}\frac{\partial^2}{\partial\theta_i\partial\theta_j}\chi_{n+1} = &\left(\frac{\partial^2}{\partial\theta_i\partial\theta_j}U_n\right)\chi_n + \left(\frac{\partial}{\partial\theta_j}U_n\right)\frac{\partial}{\partial\theta_i}\chi_n \\ &+\left(\frac{\partial}{\partial\theta_i}U_n\right)\frac{\partial}{\partial\theta_j}\chi_n + U_n\frac{\partial^2}{\partial\theta_i\partial\theta_j}\chi_n.\end{aligned} \tag{5}$$

To calculate the derivatives for each time slice one solves [67]

$$\frac{d}{d\eta}e^{\chi(\eta)} = \int_0^1 e^{\alpha\chi(\eta)}\frac{d\chi(\eta)}{d\eta}e^{(1-\alpha)\chi(\eta)}d\alpha, \tag{6}$$

which has a known solution in terms of the eigenvalues of χ [13,14,64]. Further steps in the derivation are given in the Supplemental Material [54].

Comparison to Monte Carlo simulations.—We consider here a two-level Hamiltonian given by ($\hbar = 1$)

$$H(t) = \Delta\hat{Z} + \Omega_{\max}u(t)\hat{X}, \tag{7}$$

with detuning $\Delta = 0$, maximum amplitude $\Omega_{\max}$, Pauli operators $\hat{X}$ and $\hat{Z}$, and dimensionless control function $-1 \leq u(t) \leq +1$. We consider a state transfer $|0\rangle \to |1\rangle$ where the dynamical evolution is subject to uncertainties in the system parameters $\Omega_{\max}$ and Δ. The transfer itself is induced by a Gaussian π pulse [Fig. 1(a)]. We time evolve the system for $T = 6/\Omega_{\max}$ with independent uncertainties $\sigma(\Omega_{\max})/\Omega_{\max} = \sigma(\Delta)/\Omega_{\max} = 3.0 \times 10^{-2}$ using 10 000 Monte Carlo simulations. We calculate the average trajectory over the Pauli observable $\langle\hat{Z}\rangle$ and define the confidence interval as twice the standard deviation $\pm 2\sigma(\langle\hat{Z}\rangle)$ from the average trajectory, which we truncate between ± 1,

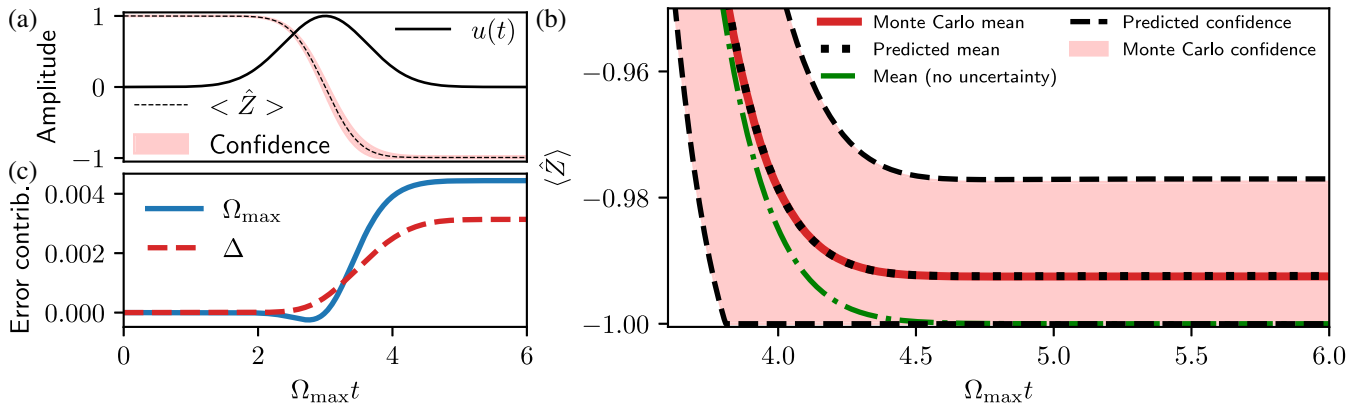

FIG. 1. Quantum uncertainty propagation when applied to a Gaussian pulse for Rabi driving [Eq. (7)]. (a) The uncertain Gaussian pulse (solid) and the result of Monte Carlo sampling (dashed line, with 2σ confidence interval shaded in red). (b) Comparison between QUPID and Monte Carlo sampling, zoomed in on later times. Here, the Monte Carlo mean (solid line) and confidence interval (shading) are shown in red, while the mean (dotted) and confidence intervals (dashed) derived from our method are plotted in black, showing excellent agreement. The mean for the uncorrected (uncertainty-free) case is shown in dash-dotted green. (c) The time-dependent error contribution to the total error (from all sources) resulting from uncertainty in the maximum drive amplitude $\Omega_{\max}$ (blue, solid) and detuning Δ (red, dashed), respectively.

as this is a physical limitation on $\langle \hat{Z} \rangle$ [Fig. 1(a)]. We compare the predictions of QUPID, Eqs. (2) and (3), to the Monte Carlo simulations by zooming in on the end of the trajectory in Fig. 1(b). Here we calculate the variance as $\mathrm{Var}[Z] = (1/N)\sum_{j=1}^{N}(Z - \bar{Z})^2$. From the figure, we see how uncertainties in the system parameters induce a shift in the mean value away from the ideal, uncertainty-less case $\langle \hat{Z} \rangle = -1$. In addition, we see excellent agreement between the Monte Carlo simulations and QUPID. On a standard laptop computer, the Monte Carlo simulations take ≈30 min, whereas QUPID takes ≈0.2 sec, providing a significant speed up.

An additional benefit of QUPID over Monte Carlo methods is that Eq. (2) allows us to directly track how each uncertainty parameter influences the system dynamics. To this end, we may define the error contribution for each parameter as $\frac{1}{2}(\partial^2\langle \hat{Z} \rangle/\partial\theta^2)\sigma(\theta)^2$ with $\theta = \Omega_{\max}, \Delta$. We plot in Fig. 1(c) the error contribution for each parameter along the trajectory. Interestingly, we see that around halfway through the trajectory, the error contributions from the amplitude and detuning are opposite in sign and thus cancel each other out to some extent; such fortuitous cancellations can be analyzed and exploited when designing pulse sequences using our method. We also see at the end of the trajectory that the two error contributions converge on different specific values. This analysis is useful in determining, e.g., which parameters are most sensitive in an experiment and thus where efforts must be concentrated when improving the precision of experimental systems.

Experimental comparison.—We compare the predictions of QUPID to a single-qubit experiment via pulse-level control of IBM's *ibmq_armonk* single-qubit system accessible via Qiskit pulse [68–70]. Such pulse-level control has previously been used to optimize the fidelity of cross-resonance gates [29], the CV gate [71], and to build a quantum compiler implementing basis gates and qudit operations [72].

First, we determine Gaussian and composite BB1 [34] pulse sequences that drive $\pi/2$ (Hadamard) and π (bit-flip) transitions. After calibration (see Supplemental Material [54]), we artificially add amplitude noise to each aforementioned pulse sequence, sampled from a Gaussian distribution centered around the optimal amplitudes with width $\epsilon = \sigma(\Omega_{\max})/\Omega_{\max}$ for $\Theta = \pi/2$ and π [73]. We compare the predictions of our theory to the experimental results in Fig. 2 with $\epsilon = 0.05$ for Gaussian and BB1 π and $\pi/2$ pulses. The data and simulations match well throughout the duration of the pulses for both cases, although our theory cannot fully account for measured BB1 errors at the final time due to discrimination or shot noise (see blue error bars) being larger than the BB1 final error, which has intrinsic robustness up to sixth order in amplitude error [34,36]. To determine how the error scales with ϵ, we compare the experimental data and theoretical predictions for the final expectation value $\langle \hat{Z} \rangle$ of a Gaussian $\pi/2$ pulse in the inset of Fig. 2(c), where we again obtain excellent agreement between theory and experiment. Thus, when compared with experimental data, our theory can determine at what point various experimental uncertainties dominate the error, which can be useful for experimental debugging, theoretical model building, or designing new systems. Moreover, by calibrating to the exact value of ϵ in the model, one can readily use Eq. (2) to remove the correction term coming from uncertainty and thereby estimate the true model parameters, e.g., for Hamiltonian learning or quantum sensing.

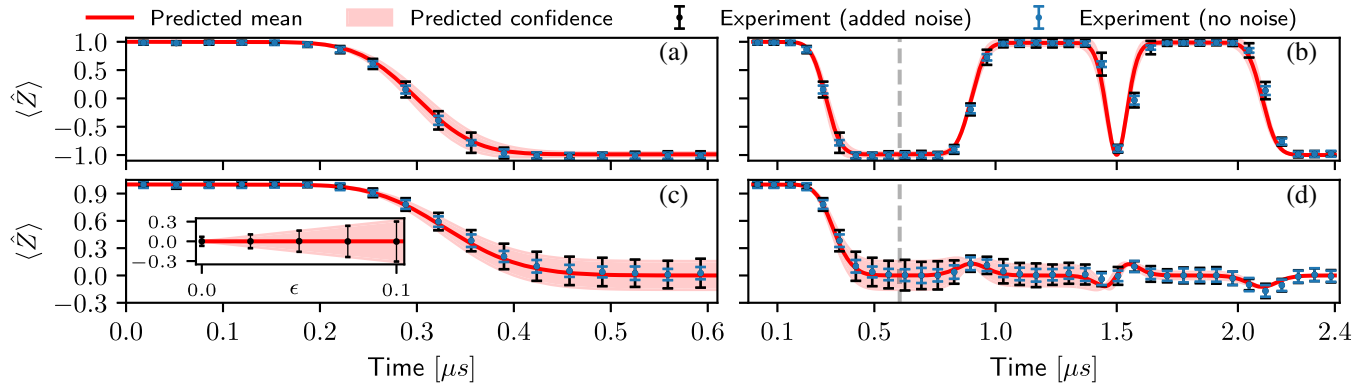

FIG. 2. Comparison of QUPID to experimental results using the IBM Armonk qubit showing how the uncertainty changes over time for a Gaussian (a) and BB1 (b) π pulse and a Gaussian (c) and BB1 (d) $\pi/2$ pulse. The black points (error bars) denote the uncertainty (twice the standard deviation on the mean) for 50 experimental runs, where for each run, we sample the amplitude from a Gaussian of width $\epsilon = 0.05$. The blue points and error bars were generated from data taken with a constant amplitude, i.e., $\epsilon = 0$. Each experimental run averages over 1024 measurements. The theoretical BB1 uncertainty goes to zero at the end points since the BB1 pulses are robust up to sixth-order error, but otherwise we obtain excellent agreement between theory and experiment when the amplitude uncertainty errors dominate over other errors in the system, e.g., measurement errors. The inset in (c) compares the predictions of the final expectation value $\langle Z \rangle$ to experimental data with respect to changes in the amplitude error ϵ for a Gaussian $\pi/2$ pulse.

Scaling and speed up.—Here, we consider how QUPID scales with the number of parameters compared to Monte Carlo simulations. Estimating the mean via Eq. (2) scales linearly (quadratically) with independent (dependent) parameters. The statistical uncertainty from Monte Carlo averaging over N samples is given by the standard deviation of the mean $\bar{\sigma} = \sigma/\sqrt{N}$ which we may estimate using Eq. (3). Hence, Monte Carlo simulations also scale linearly (quadratically) with independent (dependent) parameters.

However, in practice, many of the mixed derivatives in Eq. (3) are zero, leading Monte Carlo simulation to have an effective sublinear (subquadratic) scaling with independent (dependent) parameters. Thus, we should compare the precision of the two methods over a wide range of uncertainty parameters. We consider the spin-star system illustrated in the top right of Fig. 3, which consists of 5 qubits with interactions between the nearest and the next-nearest qubits and an external, global $\hat{X}$ control. The Hamiltonian for the spin-star system is

$$H = -\sum_{\langle i,j \rangle} \sum_{k=x,y,z} J_k^{(i,j)} \sigma_i^{(k)} \sigma_j^{(k)} - \sum_{\langle\langle i,j \rangle\rangle} \sum_{k=x,y,z} g_k^{(i,j)} \sigma_i^{(k)} \sigma_j^{(k)} + u(t) \sum_j \sigma_j^{(x)}, \quad (8)$$

where $\langle , \rangle$ and $\langle\langle , \rangle\rangle$ denotes the sum over nearest and next-nearest qubits, with couplings $J = J_k^{(i,j)}$ and $g = g_k^{(i,j)} = J/10$ for $k = x$, y, and z, respectively, giving 30 different parameters. From the initial state $|\psi_0\rangle = |00000\rangle$, we time evolve the system with a control $u(t) = \phi_1(t) + \phi_3(t) - \phi_5(t)$, where $\phi_n(t) = \sin(n\pi t/T)$ for a total duration $TJ = 10$. In the absence of uncertainties this leads to a final state $|\tilde{\psi}\rangle = |\psi(T)\rangle$ that populates a wide range of different Fock states in the Hilbert space.

We investigate how uncertainties in the system parameters induce population in states other than $|\tilde{\psi}\rangle$ quantized by the fidelity $F = \langle P \rangle$, with $P = |\tilde{\psi}\rangle\langle\tilde{\psi}|$ denoting the projector onto the state $|\tilde{\psi}\rangle$. We model normally distributed uncertainties $\sigma(J)/J = \sigma(g)/g = 0.01$ in 1, 10, 20, and 30 parameters chosen at random, where we perform 100 000

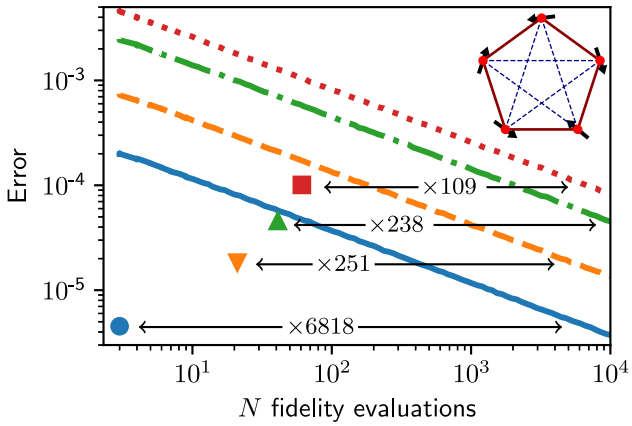

FIG. 3. Simulation results with the spin-star system (top right inset). The lines depict the expected error of Monte Carlo simulations as a function of the number of fidelity evaluations for 1 (blue solid), 10 (orange dashed), 20 (green, dash-dotted), and 30 (red dotted) parameters. This is compared to QUPID for 1 (blue circle), 10 (orange, down triangle), 20 (green, up triangle), and 30 (red square) parameter(s) chosen at random, where the computational expense has been evaluated with respect to a finite difference scheme. The horizontal arrows mark the speed improvement in an equal-accuracy comparison.

Monte Carlo simulations for each choice. To understand the scaling of Monte Carlo, we compare the difference between the fidelity average over the 100 000 samples (F_{true}) versus averages over a subset of N samples ranging from 1 to 10 000 (F_{approx}). We calculate F_{approx} by drawing N fidelities at random to evaluate the estimation error $\bar{E} = |F_{\text{true}} - F_{\text{approx}}|$. To obtain an accurate estimate for $\bar{E}$, we repeat this procedure 10 000 times. We depict the results in Fig. 3 for different numbers of uncertainty parameters. We note the $N^{-1/2}$ scaling with sample number, consistent with the standard deviation of the mean but at different heights due to different standard deviations.

We compare the performance of QUPID to Monte Carlo simulations in both accuracy and computational expense. The latter is achieved by comparing the number of fidelity evaluations required by QUPID via a finite difference scheme (see Supplemental Material [54]). Since fidelity evaluation is by far the most expensive step in each approach, this gives an accurate comparison. We plot the QUPID results in Fig. 3 as individual data points. Its relative speed up over Monte Carlo in an equal-accuracy comparison is obtainable by considering the distance from the individual data points in Fig. 3 to the lines along the x axis. For clarity, we have indicated the factor of speed up with arrows on the figure, which ranges from 6818 for one parameter to 109 for 30 parameters. Note that the relative speed up grows smaller with the number of parameters due to the sublinear Monte Carlo scaling. This implies that for a large enough number of uncertainty parameters, Monte Carlo is preferable. From the presented data, we estimate the breakeven point for the two methods to be in between 35 to 50 parameters for this particular problem. An interesting alternative for few parameters is quasi-Monte Carlo [74], which is designed for numerical integration [75] but may eventually find use in simulation methods. For this reason, we have benchmarked our methods relative to Monte Carlo methods, the standard in the field [15,18–28].

Outlook.—We have demonstrated QUPID, a method for analytically incorporating and propagating uncertainties during quantum dynamical evolution. For a reasonable ($\approx$10) number of parameters, this method scales dramatically better than Monte Carlo sampling, the method commonly used in the literature. QUPID has the additional advantages of (a) separating the role of different error sources and (b) showing how uncertainties develop over time. This can be useful for theoretical protocol improvement as well as experimental design and debugging. That is, with an understanding of the dominant uncertainty sources in a given protocol, experimentalists can better understand the level of precision that must be reached in their system and which parameters are most likely to cause imprecisions. Likewise, these analytical forms allow the design of protocols (e.g., pulse sequences) that can increase or decrease the effect of parameter uncertainty, which is useful for increased robustness or improved sensing, respectively.

We acknowledge the use of IBM Quantum services for this work. The views expressed are those of the authors, and do not reflect the official policy or position of IBM or the IBM Quantum team. This work was funded by the Carlsberg Foundation, by the Deutsche Forschungsgemeinschaft (DFG, German Research Foundation) under Germany's Excellence Strategy—Cluster of Excellence Matter and Light for Quantum Computing (ML4Q) EXC 2004/1—390534769, and through the European Union's Horizon 2020 research and innovation programme under Grant Agreements No. 817482 (PASQuanS) and No. 820394 (ASTERIQS). The numerical results presented in this work were obtained at the Centre for Scientific Computing, Aarhus.

*f.motzoi@fz-juelich.de

[1] L. K. Grover, A fast quantum mechanical algorithm for database search, in *Proceedings of the Twenty-Eighth Annual ACM Symposium on Theory of Computing* (Association for Computing Machinery, New York, 1996), pp. 212–219, 10.1145/237814.237866.

[2] P. W. Shor, Polynomial-time algorithms for prime factorization and discrete logarithms on a quantum computer, SIAM Rev. **41**, 303 (1999).

[3] J. T. Barreiro, M. Müller, P. Schindler, D. Nigg, T. Monz, M. Chwalla, M. Hennrich, C. F. Roos, P. Zoller, and R. Blatt, An open-system quantum simulator with trapped ions, Nature (London) **470**, 486 (2011).

[4] I. Bloch, J. Dalibard, and S. Nascimbene, Quantum simulations with ultracold quantum gases, Nat. Phys. **8**, 267 (2012).

[5] A. Das and B. K. Chakrabarti, Colloquium: Quantum annealing and analog quantum computation, Rev. Mod. Phys. **80**, 1061 (2008).

[6] C. C. McGeoch, Adiabatic quantum computation and quantum annealing: Theory and practice, Synth. Lect. Quantum Comput. **5**, 1 (2014).

[7] M. Schuld, I. Sinayskiy, and F. Petruccione, An introduction to quantum machine learning, Contemp. Phys. **56**, 172 (2015).

[8] J. Biamonte, P. Wittek, N. Pancotti, P. Rebentrost, N. Wiebe, and S. Lloyd, Quantum machine learning, Nature (London) **549**, 195 (2017).

[9] A. Acín, I. Bloch, H. Buhrman, T. Calarco, C. Eichler, J. Eisert, D. Esteve, N. Gisin, S. J. Glaser, F. Jelezko *et al.*, The European quantum technologies roadmap, New J. Phys. **20**, 080201 (2018).

[10] J. Taylor, *Introduction to Error Analysis, the Study of Uncertainties in Physical Measurements* (University Science Books, Sausalito, CA, 1997).

[11] N. Khaneja, T. Reiss, C. Kehlet, T. Schulte-Herbrüggen, and S. J. Glaser, Optimal control of coupled spin dynamics: Design of NMR pulse sequences by gradient ascent algorithms, J. Magn. Reson. **172**, 296 (2005).

[12] F. Motzoi, J. M. Gambetta, S. T. Merkel, and F. K. Wilhelm, Optimal control methods for rapidly time-varying Hamiltonians, Phys. Rev. A **84**, 022307 (2011).
[13] P. de Fouquières, S. G. Schirmer, S. J. Glaser, and I. Kuprov, Second order gradient ascent pulse engineering, J. Magn. Reson. **212**, 412 (2011).
[14] M. Dalgaard, F. Motzoi, J. H. M. Jensen, and J. Sherson, Hessian-based optimization of constrained quantum control, Phys. Rev. A **102**, 042612 (2020).
[15] V. Langrock and D. P. DiVincenzo, A reset-if-leaked procedure for encoded spin qubits, arXiv:2012.09517.
[16] J. J. Sørensen, J. S. Nyemann, F. Motzoi, J. Sherson, and T. Vosegaard, Optimization of pulses with low bandwidth for improved excitation of multiple-quantum coherences in NMR of quadrupolar nuclei, J. Chem. Phys. **152**, 054104 (2020).
[17] X. Ge, H. Ding, H. Rabitz, and R.-B. Wu, Robust quantum control in games: An adversarial learning approach, Phys. Rev. A **101**, 052317 (2020).
[18] R. Vieira and G. Rigolin, Almost perfect transmission of multipartite entanglement through disordered and noisy spin chains, Phys. Lett. A **384**, 126536 (2020).
[19] W. Song, J. Ryu, K. Baek, and J. Bang, Average fidelity and fidelity deviation in noisy quantum teleportation, J. Korean Phys. Soc. **78**, 496 (2021).
[20] M. P. Estarellas, T. P. Spiller, and I. D'Amico, Comparison of entangling protocols in ABC-type spin chains, J. Phys.: Conf. Ser. **1638**, 012013 (2020).
[21] D. S. A. Coden, S. S. Gómez, A. Ferrón, and O. Osenda, Controlled quantum state transfer in XX spin chains at the quantum speed limit, Phys. Lett. A **387**, 127009 (2021).
[22] J. Cabedo, J. Claramunt, and A. Celi, Dynamical preparation of stripe states in spin-orbit-coupled gases, Phys. Rev. A **104**, L031305 (2021).
[23] A. Kiely and S. Campbell, Fast and robust magnon transport in a spin chain, New J. Phys. **23**, 033033 (2021).
[24] F. M. D'Angelis, F. A. Pinheiro, D. Guéry-Odelin, S. Longhi, and F. Impens, Fast and robust quantum state transfer in a topological Su-Schrieffer-Heeger chain with next-to-nearest-neighbor interactions, Phys. Rev. Research **2**, 033475 (2020).
[25] F. A. Calderon-Vargas, E. Barnes, and S. E. Economou, Fast high-fidelity single-qubit gates for flip-flop qubits in silicon, arXiv:2101.11592.
[26] J.-L. Wu, Y. Wang, J.-X. Han, S.-L. Su, Y. Xia, Y. Jiang, and J. Song, Resilient quantum gates on periodically driven Rydberg atoms, Phys. Rev. A **103**, 012601 (2021).
[27] G. L. Giorgi, S. Lorenzo, and S. Longhi, Topological protection and control of quantum Markovianity, Photonics **7**, 18 (2020).
[28] S. Hu, Y. Ke, and C. Lee, Topological quantum transport and spatial entanglement distribution via a disordered bulk channel, Phys. Rev. A **101**, 052323 (2020).
[29] S. Sheldon, E. Magesan, J. M. Chow, and J. M. Gambetta, Procedure for systematically tuning up cross-talk in the cross-resonance gate, Phys. Rev. A **93**, 060302(R) (2016).
[30] L. S. Theis, F. Motzoi, S. Machnes, and F. K. Wilhelm, Counteracting systems of diabaticities using DRAG controls: The status after 10 years, Europhys. Lett. **123**, 60001 (2018).
[31] A. D. Patterson, J. Rahamim, T. Tsunoda, P. A. Spring, S. Jebari, K. Ratter, M. Mergenthaler, G. Tancredi, B. Vlastakis, M. Esposito, and P. J. Leek, Calibration of a Cross-Resonance Two-Qubit Gate Between Directly Coupled Transmons, Phys. Rev. Applied **12**, 064013 (2019).
[32] E. Magesan and J. M. Gambetta, Effective Hamiltonian models of the cross-resonance gate, Phys. Rev. A **101**, 052308 (2020).
[33] N. Sundaresan, I. Lauer, E. Pritchett, E. Magesan, P. Jurcevic, and J. M. Gambetta, Reducing unitary and spectator errors in cross resonance with optimized rotary echoes, PRX Quantum **1**, 020318 (2020).
[34] S. Wimperis, Broadband, narrowband, and passband composite pulses for use in advanced NMR experiments, J. Magn. Reson., Ser. A **109**, 221 (1994).
[35] H. K. Cummins, G. Llewellyn, and J. A. Jones, Tackling systematic errors in quantum logic gates with composite rotations, Phys. Rev. A **67**, 042308 (2003).
[36] L. M. K. Vandersypen and I. L. Chuang, NMR techniques for quantum control and computation, Rev. Mod. Phys. **76**, 1037 (2005).
[37] M. Möttönen, R. de Sousa, J. Zhang, and K. B. Whaley, High-fidelity one-qubit operations under random telegraph noise, Phys. Rev. A **73**, 022332 (2006).
[38] T. W. Borneman, M. D. Hürlimann, and D. G. Cory, Application of optimal control to CPMG refocusing pulse design, J. Magn. Reson. **207**, 220 (2010).
[39] T. E. Skinner, M. Braun, K. Woelk, N. I. Gershenzon, and S. J. Glaser, Design and application of robust rf pulses for toroid cavity NMR spectroscopy, J. Magn. Reson. **209**, 282 (2011).
[40] F. Motzoi, E. Halperin, X. Wang, K. B. Whaley, and S. Schirmer, Backaction-driven, robust, steady-state long-distance qubit entanglement over lossy channels, Phys. Rev. A **94**, 032313 (2016).
[41] F. Platzer, F. Mintert, and A. Buchleitner, Optimal Dynamical Control of Many-Body Entanglement, Phys. Rev. Lett. **105**, 020501 (2010).
[42] M. M. Müller, S. Gherardini, T. Calarco, S. Montangero, and F. Caruso, Information theoretical limits for quantum optimal control solutions: Error scaling of noisy channels, arXiv:2006.16113.
[43] S. Lloyd and S. Montangero, Information Theoretical Analysis of Quantum Optimal Control, Phys. Rev. Lett. **113**, 010502 (2014).
[44] J. Koch, T. M. Yu, J. Gambetta, A. A. Houck, D. I. Schuster, J. Majer, A. Blais, M. H. Devoret, S. M. Girvin, and R. J. Schoelkopf, Charge-insensitive qubit design derived from the cooper pair box, Phys. Rev. A **76**, 042319 (2007).
[45] C. Rigetti and M. Devoret, Fully microwave-tunable universal gates in superconducting qubits with linear couplings and fixed transition frequencies, Phys. Rev. B **81**, 134507 (2010).
[46] M. H. Goerz, F. Motzoi, K. B. Whaley, and C. P. Koch, Charting the circuit QED design landscape using optimal control theory, npj Quantum Inf. **3**, 37 (2017).
[47] P. Brooks, A. Kitaev, and J. Preskill, Protected gates for superconducting qubits, Phys. Rev. A **87**, 052306 (2013).

[48] T. Menke, F. Häse, S. Gustavsson, A. J. Kerman, W. D. Oliver, and A. Aspuru-Guzik, Automated design of superconducting circuits and its application to 4-local couplers, npj Quantum Inf. **7**, 49 (2021).
[49] L. B. Nguyen, Y.-H. Lin, A. Somoroff, R. Mencia, N. Grabon, and V. E. Manucharyan, High-Coherence Fluxonium Qubit, Phys. Rev. X **9**, 041041 (2019).
[50] Note that the expression we derive for the mean works for any symmetric distribution.
[51] G.-C. Wick, The evaluation of the collision matrix, Phys. Rev. **80**, 268 (1950).
[52] L. Isserlis, On a formula for the product-moment coefficient of any order of a normal frequency distribution in any number of variables, Biometrika **12**, 134 (1918).
[53] See the section *Calculation of Mean and Variance* in the Supplemental Material [54], which includes Refs. [51,52,55–59].
[54] See Supplemental Material at http://link.aps.org/supplemental/10.1103/PhysRevLett.128.150503 for more detailed derivation of the mean and variance, a description of how the required derivatives can be calculated numerically, some further experimental details, and an application of our method to a classical damped pendulum.
[55] V. Leonov and A. N. Shiryaev, On a method of calculation of semi-invariants, Theory Probab. Appl. **4**, 319 (1959).
[56] T. Linder, Moment generating functions and multivariate normal distribution (lecture slides) (2017), https://mast.queensu.ca/~stat353/slides/5-multivariate_normal17_4.pdf.
[57] M. G. Kendall, *The Advanced Theory of Statistics* (Charles Griffin and Company Limited, London, 1945). Vol. 1.
[58] J. Marcinkiewicz, Sur une propriété de la loi de Gauß, Math. Z. **44**, 612 (1939).
[59] A. Rajagopal and E. Sudarshan, Some generalizations of the Marcinkiewicz theorem and its implications to certain approximation schemes in many-particle physics, Phys. Rev. A **10**, 1852 (1974).
[60] D. L. Goodwin and I. Kuprov, Modified Newton-Raphson GRAPE methods for optimal control of spin systems, J. Chem. Phys. **144**, 204107 (2016).
[61] B. Fornberg, Generation of finite difference formulas on arbitrarily spaced grids, Math. Comput. **51**, 699 (1988).
[62] J. H. M. Jensen, F. S. Møller, J. J. Sørensen, and J. F. Sherson, Approximate dynamics leading to more optimal control: Efficient exact derivatives, Phys. Rev. A **103**, 062612 (2021).
[63] See the section *Numerical Calculation of Derivatives* in the Supplemental Material [54], which includes Refs. [11,13,14,61,64,65].
[64] S. Machnes, U. Sander, S. J. Glaser, P. de Fouquières, A. Gruslys, S. Schirmer, and T. Schulte-Herbrüggen, Comparing, optimizing, and benchmarking quantum-control algorithms in a unifying programming framework, Phys. Rev. A **84**, 022305 (2011).
[65] C. Navarrete-Benlloch, Open systems dynamics: Simulating master equations in the computer, arXiv:1504.05266.
[66] S. Blanes, F. Casas, J.-A. Oteo, and J. Ros, The Magnus expansion and some of its applications, Phys. Rep. **470**, 151 (2009).
[67] R. M. Wilcox, Exponential operators and parameter differentiation in quantum physics, J. Math. Phys. (N.Y.) **8**, 962 (1967).
[68] D. C. McKay *et al.*, Qiskit backend specifications for OpenQASM and OpenPulse experiments, arXiv:1809.03452v1.
[69] T. Alexander, N. Kanazawa, D. J. Egger, L. Capelluto, C. J. Wood, A. Javadi-Abhari, and D. C. McKay, Qiskit pulse: Programming quantum computers through the cloud with pulses, Quantum Sci. Technol. **5**, 044006 (2020).
[70] T. Alexander, N. Kanazawa, D. J. Egger, L. Capelluto, C. J. Wood, A. Javadi-Abhari, and D. C McKay, Qiskit pulse: Programming quantum computers through the cloud with pulses, Quantum Sci. Technol. **5**, 044006 (2020).
[71] S. Oomura, T. Satoh, M. Sugawara, and N. Yamamoto, Design and application of high-speed and high-precision CV gate on IBM Q OpenPulse system, arXiv:2102.06117.
[72] P. Gokhale, A. Javadi-Abhari, N. Earnest, Y. Shi, and F. T. Chong, Optimized quantum compilation for near-term algorithms with OpenPulse, in *Proceedings of the 2020 53rd Annual IEEE/ACM International Symposium on Microarchitecture (MICRO)* (IEEE, Athens, Greece, 2020), pp. 186–200, 10.1109/MICRO50266.2020.00027.
[73] For the qubit drive times considered here, the intrinsic qubit errors, e.g., due to relaxation, are negligible, so this system is a suitable playground for the artificially inserted uncertainties that can be used to test our theory.
[74] M. Maček, P. T. Dumitrescu, C. Bertrand, B. Triggs, O. Parcollet, and X. Waintal, Quantum Quasi-Monte Carlo Technique for Many-Body Perturbative Expansions, Phys. Rev. Lett. **125**, 047702 (2020).
[75] R. E. Caflisch, Monte Carlo and quasi-Monte Carlo methods, Acta Numer. **7**, 1 (1998).